Bull Volcanol (2015) 77: 15
DOI 10.1007/s00445-015-0901-7

RESEARCH ARTICLE

Experiments with vertically and laterally migrating subsurface explosions with applications to the geology of phreatomagmatic and hydrothermal explosion craters and diatremes

Greg A. Valentine · Alison H. Graettinger · Élodie Macorps · Pierre-Simon Ross · James D. L. White · Erika Döhring · Ingo Sonder

Received: 21 October 2014 / Accepted: 12 January 2015 / Published online: 7 February 2015

Abstract We present results of experiments that use small chemical explosive charges buried in layered aggregates to simulate the effects of subsurface hydrothermal and phreatomagmatic explosions at varying depths and lateral locations, extending earlier experimental results that changed explosion locations only along a vertical axis. The focus is on the resulting crater size and shape and subcrater structures. Final crater shapes tend to be roughly circular if subsurface explosion epicenters occur within each other's footprints (defined as the plan view area of reference crater produced by a single explosion of a given energy, as predicted by an empirical relationship). Craters are elongate if an epicenter lies somewhat beyond the footprint of the previous explosion, such that their footprints overlap, but if epicenters are too far apart, the footprints do not overlap and separate craters result. Explosions beneath crater walls formed by previous blasts tend to produce inclined (laterally directed) ejecta jets, while those beneath crater centers are vertically focused. Lateral shifting of explosion sites results in mixing of subcrater materials by development of multiple subvertical domains of otherwise pure materials, which progressively break down with repeated blasts, and by ejection and fallback of deeper-seated material that had experienced net upward displacement to very shallow levels by previous explosions. A variably developed collar of material that experienced net downward displacement surrounds the subvertical domains. The results demonstrate key processes related to mixing and ejection of materials from different depths during an eruptive episode at a maar-diatreme volcano as well as at other phreatomagmatic and hydrothermal explosion sites.

Keywords Phreatomagmatic · Hydrothermal explosion · Crater · Ejecta · Diatreme · Maar · Phreatic · Kimberlite pipe

Editorial responsibility: S. Self, acting Executive Editor

Electronic supplementary material The online version of this article (doi:10.1007/s00445-015-0901-7) contains supplementary material, which is available to authorized users.

G. A. Valentine (✉) · A. H. Graettinger · É. Macorps · I. Sonder
Department of Geology and Center for Geohazards Studies, State University of New York, 411 Cooke Hall, Buffalo, NY 14260, USA
e-mail: gav4@buffalo.edu

É. Macorps
Laboratoire Magmas et Volcans, Observatoire de Physique du Globe de Clermont-Ferrand, Université Blaise Pascal, 5 rue Kessler, 63038 Clermont-Ferrand, France

P.-S. Ross
Institut National de la Recherche Scientifique, Centre Eau Terre Environnement, 490 rue de la Couronne, Québec Québec G1K 9A9, Canada

J. D. L. White
Geology Department, University of Otago, P.O. Box 56, Dunedin 9054, New Zealand

E. Döhring
Institut Polytechnique LaSalle Beauvais, 19 rue Pierre Waguet, 60000 Beauvais, France

Introduction

Many subaerial volcanoes experience some form of hydrothermal or/and phreatomagmatic, subsurface explosions during their lifetimes. For example, hydrothermal explosions (sometimes referred to as phreatic explosions), involving steam but no juvenile magma, are common during unrest at composite volcanoes (e.g., Mount St. Helens in 1980 and Soufrière Hills,

Montserrat, in 1995; Christiansen and Peterson 1981; Kokelaar 2002) or can be triggered by events such as landslides that are unrelated to broader unrest but that rapidly unload a pressurized hydrothermal system (e.g., Procter et al. 2014). Phreatomagmatic explosions, which involve direct interaction of magma and water, can form one of the most common subaerial volcanic crater types, referred to as maars, along with their surrounding tephra (ejecta) rings. The subcrater structures beneath maar volcanoes (diatremes) commonly preserve features inferred to be the direct products of subsurface phreatomagmatic explosions. Lab- and field-scale experiments exploring the relations between crater and diatreme features and subsurface explosions have focused mainly on the effects of single explosions or explosions that migrate vertically (Ross et al. 2008a; b; Valentine et al. 2012; Ross et al. 2013; Andrews et al. 2014; Graettinger et al. 2014). Downward migration of explosion sites is commonly invoked to explain the presence of progressively deeper-seated country rock lithic clasts in the upper parts of tephra ring stratigraphy (Lorenz 1986), although recent work indicates that this migration is not a simple progressive deepening but, instead, involves less predictable variations in explosion depth (e.g., White and McClintock 2001; Ross and White 2006; White and Ross 2011; Valentine and White 2012; Valentine 2012; LeFebvre et al. 2013).

Hydrothermal and phreatomagmatic explosion vent areas commonly preserve evidence of multiple explosions that also migrated laterally. Evidence includes lines or clusters of closely spaced craters, which may coalesce with continued activity and crater growth to form a single large crater with scalloped margins and/or a complex shape, along with nested craters with different depths (e.g., Begét et al. 1996). Ballistics analysis of ejecta blocks and detailed mapping of tephra ring deposits may reveal additional evidence of multiple explosion epicenters during a single active episode (e.g., Carrasco-Núñez et al. 2007; Ort and Carrasco-Núñez 2009; Jordan et al. 2013; van Otterloo et al. 2013; Breard et al. 2014). Diatremes, including kimberlite pipes, also show evidence of both vertically and laterally shifting explosion sites in the form of irregularly shaped, subvertical columns of pyroclasts and lithic clasts that maintain consistent internal composition compared to adjacent materials (Fig. 1; e.g., Ross and White 2006; Brown et al. 2008; LeFebvre et al. 2013; Delpit et al. 2014); the columns are inferred by some of these authors to record emplacement of material by explosion-driven debris jets.

Here, we present results of experiments that explore some aspects of both laterally and vertically shifting explosions, using small chemical explosive charges buried in layered aggregates to simulate the effects of subsurface hydrothermal or/and phreatomagmatic explosions. First, we briefly review experiments with vertical-only migration from previous tests and a new experiment, to provide a basis for comparison. Then, we focus in detail on the effects of lateral and of combined vertical and lateral, migration of explosions, specifically assessing crater size and shape and subcrater structures. The data reveal relations between the distance between explosion epicenters and the resulting crater(s) shape. Explosions

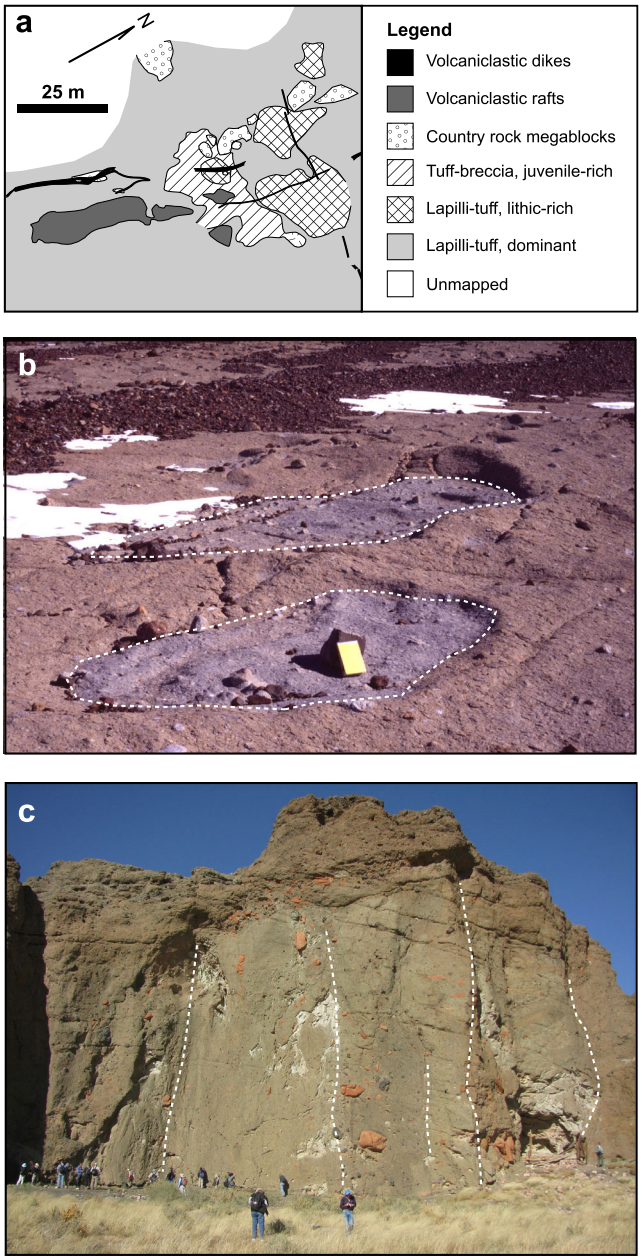

Fig. 1 Field examples of unbedded diatremes containing multiple adjacent, mutually crosscutting zones of pyroclastic rocks with contrasting componentry and/or grain size, with the zones having steep to vertical contacts with one another. We interpret these columnar features as reflecting the passage of multiple debris jets in the diatreme, from laterally and vertically migrating explosions sites. **a**, **b** Subhorizontal outcrops from a diatreme complex at Coombs Hills, Antarctica, showing the circular, elliptic, or irregular shapes of the columnar zones in map view. See Ross and White (2006) for more details. In **b**, the *yellow object* is a field notebook about 20 cm high. **c** Vertical outcrop at Round Butte, Hopi Buttes Volcanic Field, Arizona. The *upper part* of the outcrop has diffuse bedding, but the rest of it shows *vertical columns*, the contacts of which are noted with *white dashed lines*. People for scale. See White (1991) for more details

beneath preexisting craters can produce inclined (directed) jets that significantly affect ejecta distribution. In the subsurface, lateral shifting of explosion sites promotes mixing of material from different levels in the substrate. The overall structure of subsurface deposits, with subvertical massive domains surrounded by variably developed collars of host material that experienced net downward displacement, resembles some aspects of structures induced by fluidization—a process that has been inferred for diatremes and kimberlite pipes—but the mechanisms for producing these during discrete explosions are quite different from those related to fluidization.

Methods, blast phenomenology, and scaling

Experimental method and data collection

The basic experimental approach is described by Valentine et al. (2012), Ross et al. (2013), and Graettinger et al. (2014). For three of the four new experiments, a site—referred to as a pad—was prepared by filling a trench with a repeated sequence of 15-cm-thick, mechanically compacted layers composed of (from top down) non-cohesive sand, crushed limestone (limestone screenings, particles in the sand size range), and crushed asphalt. Remaining pore spaces in the aggregates had low water contents that did not, qualitatively, result in substantial cohesive behavior. The depth of a pad depended upon the depth of explosions planned for that particular experiment; in each case, the pad depth was 30–40 cm deeper than the deepest explosion in order to minimize boundary effects on the explosion process. Pad dimensions were as follows (depth × width × breadth): pads 1 and 3—1.35 m × 4 m × 4 m; pad 2—0.75 m × 5 m × 4 m; and pad 4—1.35 m × 3 m × 3 m. The three-layer sequence was repeated up to three times (nine total layers) in pads 1, 2, and 3, as needed to fill their trenches to a surface level with the surrounding ground, and the surfaces of pads 1–3 were covered with a thin layer of well-sorted crushed aragonite sand to provide visual contrast between the surface and ejecta for post-blast analysis. Pad 4 was composed of a mix of 90 % sand and 10 % plaster of Paris that formed a damp, weakly cohesive substrate, with a surface layer of limestone screenings.

The explosive charges were each 12-cm-long cylinders, weighed 0.15 kg, and had an explosive energy of 7.5×10^5 J. Charge emplacement holes were made by hammering a pipe to 10–20 cm below the intended charge depth and vacuuming out the pipe contents; colored sand was then poured into the hole to until its top was 5 cm below the target depth. The charge was placed on end so that its center was at the target depth (±2 cm), then the (uncompacted) colored sand was poured around the charge to hold it in place and additionally to fill the hole up to its top. Each experiment involved separate detonation of three to six charges in a pad (Table 1). We discuss the experiments in order of complexity (pad 4, followed by 2, 3, and 1) and use a simple notation indicating pad number and blast number at that pad (e.g., P1B2 indicates pad 1, blast 2).

Two orthogonal topographic profiles were measured before and after each experiment. A rod was pushed into the pad at 20-cm intervals along the same profile lines in order to obtain qualitative information on the extent of subsurface disruption; disrupted pad materials tend to be weaker, and the rod penetrates deeper into them when a similar force is applied, compared to undisturbed materials (see Ross et al. 2013; Graettinger et al. 2014). In addition, a suite of high-resolution photographs was taken after each blast for photogrammetric analysis and construction of three-dimensional digital elevation models, which provided data for this paper such as crater dimensions and shapes. Near-field accelerometers, seismometers, acoustic and infrasound sensors, electrical field sensors, high-speed thermal infrared cameras, ejecta samplers, blast wave detectors, and an array of high-speed visible-light cameras also collected data during the blasts. These data will be presented elsewhere in papers focusing on ejecta dynamics and geophysical processes (e.g., Bowman et al. 2014).

The four pads were excavated after completion of the experimental run. Excavations produced near-vertical faces through each pad at regular intervals (~20 cm) to reveal cross sections of the craters and the subcrater structures that resulted from the blasts. Cross sections were documented by the investigators and photographed in detail. Samples were collected in key structures and were analyzed for componentry using a binocular microscope.

Blast phenomenology and scaling

Crater morphology and ejecta dynamics are largely determined by scaled depth, $D_{sc}=d \cdot E^{-1/3}$, where d is the physical depth (m) of a charge and E is the explosion energy (J); D_{sc} has units of m $J^{-1/3}$ (e.g., Houser 1969; Goto et al. 2001; Valentine et al. 2012; Graettinger et al. 2014). Optimal crater excavation (Fig. 2) occurs when $D_{sc} \approx 0.004$ m $J^{-1/3}$ or ~35 cm for the charges we used. As scaled depth increases relative to the optimal depth for a given explosion energy, excavation is progressively less efficient and resulting craters smaller, until $D_{sc} \approx 0.008$ m $J^{-1/3}$, which marks the approximate transition to full containment in the subsurface (i.e., non-eruptive explosion, Fig. 2; Valentine et al. 2014). For the charges reported here, this transition depth is ~70 cm. These values are approximate, with variability of about 20 % in the threshold values depending upon material properties, including whether a previous blast has weakened and de-compacted the host materials. Note that our experiments are not yet aimed at reproducing specific geologic settings (material properties) but at investigating general phenomena.

Subsurface blast phenomena and resulting crater sizes as functions of scaled depth are consistent, to first order, in

Table 1 Blast configurations and resulting crater dimensions

Pad number (2014 experiment series)	Charge number – depth (m)[a]	Scaled depth (m $J^{-1/3}$)[b]	Charge horizontal location diagram[c]	Final crater maximum diameter (m)[d]	Final crater minimum diameter (m)[d]	Ratio of maximum to minimum diameters	Final crater depth (m)[e]
4	1 – 0.46	0.0051	1,2,3	1.5	1.4	1.1	0.35
	2 – 0.50	0.0055	*				
	3 – 0.47	0.0052					
2	1 – 0.50	0.0055	4 3 1	2.1	1.3	1.6	0.47
	2 – 0.50	-	* * *				
	3 – 0.50	-	*				
	4 – 0.50	-	2				
3	1 – 0.80	0.0088	3 1	1.1[f]	1.0[f]	1.1[f]	0.06[f]
	2 – 0.80	0.0088	* *				
	3 – 0.80	0.0088	*2				
1	1 – 0.70	0.0077		1.9	1.5	1.2	0.57
	2 – 0.75	0.0083	3,6 1,4				
	3 – 0.75	0.0083	* *				
	4 – 0.50	0.0055	*				
	5 – 0.50	-	2,5				
	6 – 0.50	-					

[a] All values give depth with respect to undisturbed pad surface, except for pad 4, where depths for blasts 2 and 3 were measured relative to the bottom of crater from previous blasts. Depths are accurate to approximately ±0.03 m

[b] Scaled depths are not given where blast was emplaced beneath a sloping crater wall from previous blasts. All charges had energy of 7.5×10^5 J per charge

[c] Horizontal spacing between adjacent charges is 0.5 m in all cases. *Numerals* indicate charge number(s) for each location (epicenter)

[d] Measured between highest point on crater rim (including ejecta) on opposing sides of crater

[e] Depth measured from high point on rim (including ejecta) to lowest point within crater

[f] Pad 3 crater was a subsidence pit, rather than an excavated crater as in the other three pads

experiments across a wide range of explosion energies from our experiments (order ~10^6 J) to nuclear explosions (up to 10^{15} J; Ross et al. 2013) and for a range of geological host materials from hard rock to unconsolidated sediments (e.g., Rooke et al. 1974). Valentine et al. (2014) argue that most phreatomagmatic explosions in maar-diatreme volcanoes likely have energies of ~10^9–10^{13} J and occur at a range of scaled depths that include those used for the experiments reported here. Energy estimates for the large 2012 hydrothermal explosions of Te Maari (Tongariro, New Zealand) are ~10^{12}–10^{13} J (Jolly et al. 2014; Lube et al. 2014) and 4×10^9 J for a phreatic explosion in 2000 at Usu (Japan; Ohba et al. 2002). Thus, the data from chemical and nuclear explosions encompass the energies of many natural hydrothermal and phreatomagmatic explosions, ensuring that the general results of our experiments scale to those of the natural cases.

Summary of previous results and terminology

Previous experiments (Valentine et al. 2012; Taddeucci et al. 2013; Ross et al. 2013; Graettinger et al. 2014) that focused on vertical-only variation of charge depth provide a starting point for the new results here. Eruptive explosions ($D_{sc}<$ 0.008 m $J^{-1/3}$) produced excavated craters surrounded by ejecta rings and with fallback deposits on the crater floors or, in cases where D_{sc} approached the containment threshold, produced "negative craters" (retarcs) that are mounds of fallback on the explosion epicenters. Distribution and relative proportions of ejecta (defined as material deposited outside the crater) and fallback (deposited in the crater) depended upon scaled depth and whether a preexisting crater was present. Subcrater structures consisted of two main parts. The upper part typically was composed of crudely or discontinuously layered deposits that contained a mixture of clasts. Within these bedded subcrater deposits, some beds or lenses were composed of poorly mixed material from individual pad layers. All of these materials were derived from locations originally above the charge. In this paper, we use the term *mixed fallback* to refer to equivalent deposits, because bedding was less apparent for these experiments. Although inclusion of the word *fallback* in the term implies a mechanism and is not purely descriptive, the term is justified because these deposits trace continuously into the ejecta deposited around the crater and indicate that mixed fallback is the component of lofted material that did not get dispersed outside the crater. The word *mixed* is used here where materials derived from different levels within a pad are mixed at the scale of individual grains.

The lower subsurface structures were crudely concentric to irregularly shaped domains of unmixed (or slightly mixed) pad layers and are referred to as *domainal subcrater deposits*. The central cores of the deposits consisted of pad material

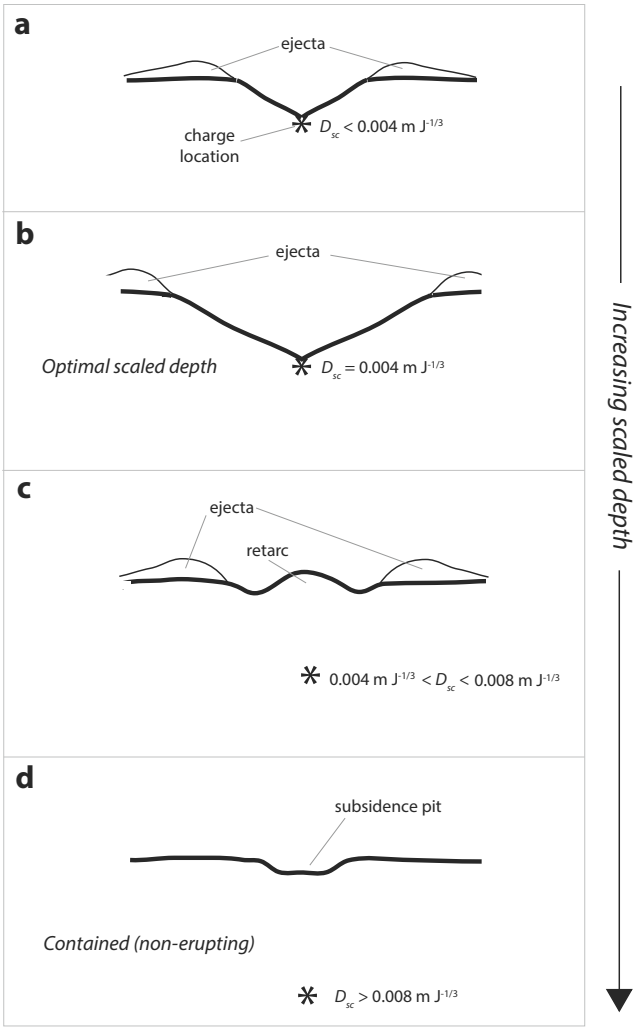

Fig. 2 Diagrammatic illustration of crater profiles for different scaled depths. *Asterisks* show explosion centers. **a** Shallower than optimal depth blast, which makes a small crater and disperses excavated materials to relatively large distances on a wide range of ballistic paths. **b** Optimal scaled depth, which excavates the largest crater. **c** At scaled depths between the optimal and containment values, craters are smaller and poor dispersal of excavated material causes much of it to fall back into the crater (in some cases forming a mound or retarc, as illustrated) and in the proximal ejecta ring. **d** At scaled depths greater than the containment threshold, no material is ejected but a subsidence pit may form at the surface

from the level of the charge and above that had been displaced upward in cases where D_{sc}<0.008 m J$^{-1/3}$ and the contacts between domains were typically irregular and subvertical. Around these cores, the pad materials were typically displaced downward compared to their original locations within pad stratigraphy. In other words, downward-displaced stratigraphy formed a collar around upward-displaced materials. Experiments with charges significantly deeper than the containment threshold (D_{sc}=0.011 m J$^{-1/3}$) produced collapse pits on the surface with no ejecta, and their subsurface structures were bowl-like domains of downward-displaced pad materials above and immediately below the charge locations. Experiments that combined non-eruptive and eruptive conditions contained elements of both subsurface structure types (Graettinger et al. 2014). Domainal subcrater deposits formed partly as material was displaced upward during development of the transient crater (Ross et al. 2013) but was not fully dismembered during expansion of explosion gasses before falling back into place with irregular and crosscutting relations and by downward displacement of materials down the sides of the transient crater (Ross et al. 2008a; b; Andrews et al. 2014). It is important to note that the fallback mechanism is important for domainal deposits, particularly in the central portions of the structures, in addition to the deposits that we specifically refer to as mixed fallback. Rod penetration profiles reveal that a disrupted zone, with reduced cohesion compared to pre-blast conditions but no visible change, extends beyond most visibly disrupted domainal deposits. Ross et al. (2013) referred to this as cryptic fallback because it also was likely lofted a small amount during the transient crater phase of a given blast. Explosions close to or below the containment threshold were progressively dominated by subsidence that formed around the transient cavities produced by explosion gasses, with decreasing degrees of lofting and fallback, and this is reflected in the domainal subcrater deposits we describe here.

Results

Below, we present results from the 2014 experiments in order of increasing complexity, starting with pad 4, which duplicated some previous vertically migrating charge configurations but with relatively homogeneous pad materials (compared to the different layers in previous work). It is included here as a point of comparison of crater morphology with no lateral blast migration. Pad 2 featured laterally migrating, eruptive explosions, while pad 3 involved lateral migration of non-eruptive blasts only slightly deeper than the containment threshold. Pad 1, the most complex, involved laterally migrating deep—but just shallower than the containment threshold—blasts followed by laterally migrating but shallower blasts.

Pad 4—vertical migration only

Pad 4 had three charges detonated beneath the same epicenter in the center of the pad (Table 1), in a configuration that duplicated that of two previous experiments in 2012 and 2013 (pad 3 in Valentine et al. 2012 and in Graettinger et al. 2014). The objective was for each charge to have a similar scaled depth with respect to the ground surface at its epicenter. After the first and second blasts, this surface was a crater floor, so the explosions were centered at progressively increasing

depths relative to the original pad surface. Each blast ejected material and had the net effect of excavating a crater (Fig. 3), but ejecta dispersal was limited and a significant portion of it fell right back into the crater, forming hummocky fallback deposits during the final blast (see especially Fig. 3c). Because of the significant fallback in the crater, its depth did not substantially increase with successive blasts even though the scaled depth was approximately constant. The phenomenon of significant direct fallback into a crater, resulting in hummocky deposits, is the combined effect of the scaled depths being deeper than the optimal excavation value (Table 1) and the vertical focusing of ejecta jets through a preexisting crater (Fig. 4a, see video at Online Resource 1; Houser 1969; Valentine et al. 2012; Taddeucci et al. 2013; Graettinger et al. 2014). The perimeter of the final crater was approximately circular (Table 1) and the upper ~15 cm of the crater wall were nearly vertical. The low point of the crater floor was offset relative to the blasts' epicenter due to the hummocky fallback deposits (Fig. 5). We do not discuss the subcrater structure here but refer the reader to Ross et al. (2013) and Graettinger et al. (2014) where a similar blast configuration was used with similarly layered materials to the other pads discussed herein.

Pad 2—lateral migration only, relatively shallow blasts

Pad 2 had four charges. The first three were arranged at the corners of an equilateral triangle with 50-cm sides, while the fourth was placed 50 cm from charge 3 in line with charges 1 and 3 (Table 1). Note that the lateral spacing of 50 cm was used for all charges at pads 1–3 in order to ensure that surface and subsurface effects of blasts were close enough to interact with structures produced by preceding blasts (as opposed to spacing them too far, which would produce independent structures). All charges were centered 50 cm below the original pad surface. The first blast (Fig. 4b, Online Resource 2) produced a crater with a hummocky fallback deposit on its floor and limited ejecta around the crater distributed in distinct rays (Fig. 6); this behavior is consistent with previous experiments with the scaled depth of ~0.006 m $J^{-1/3}$. The P2B1 crater diameter was ~118 cm; thus, the charge for blast 2 was located beneath the north-facing crater wall, and the distance from the wall to the charge was <50 cm. As a result, P2B2 produced much more ejecta than the first blast; the ejecta formed a north-tilted jet and dispersed most material in that direction. The P2B2 crater was deeper and slightly elongated parallel to the line between charges 1 and 2 (Fig. 6). Charge 3 was located beneath the east-facing wall of the P2B2 crater. Its ejecta jet was tilted eastward, and the resulting crater was elongate ENE–WSW (Fig. 6). Charge 4 was placed beneath the east-facing wall of the P2B3 crater. It again produced an east-tilted ejecta jet (Fig. 4c, Online Resource 3) and further elongated the crater along the east–west direction (Fig. 6). The final

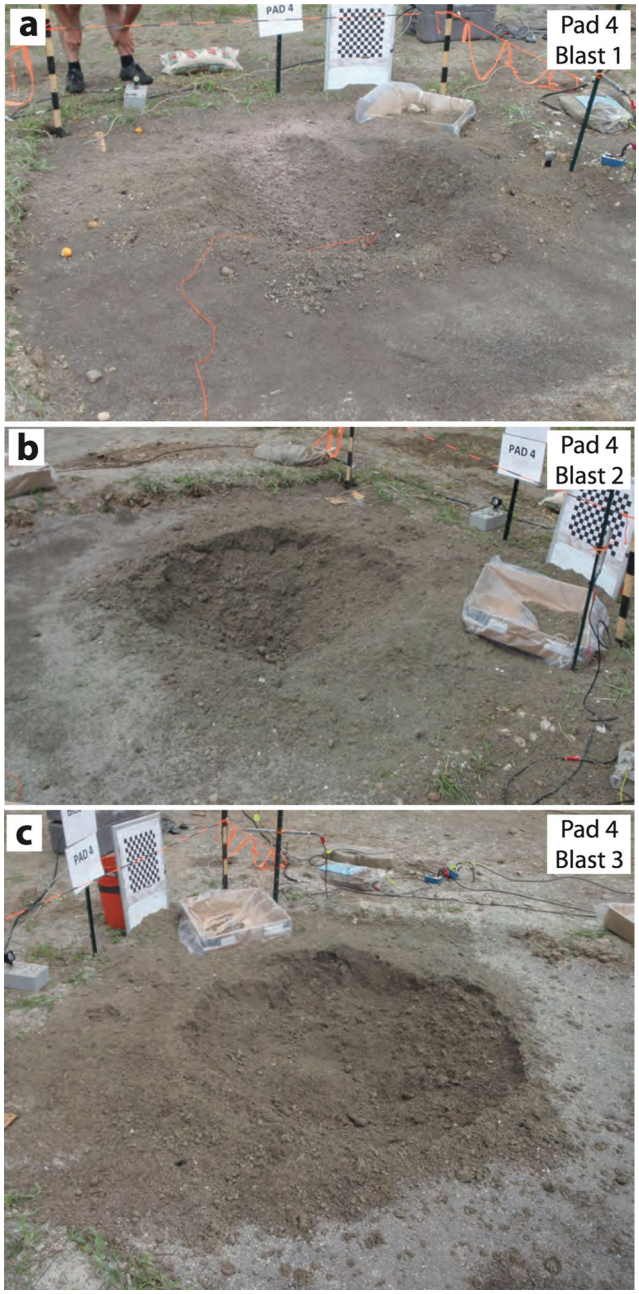

Fig. 3 Pad 4 crater after each blast: **a** blast 1, **b** blast 2, and **c** blast 3. Note asymmetry and limited extent of ejecta blanket after each explosion. Checkerboard pattern visible in photograph is 55 cm×55 cm

crater perimeter was elongate with a slight inflection on either side of the long edges, similar to nested craters in nature (Fig. 5 and Table 1). The deepest point (47 cm; Table 1) in the crater was offset from the center of the structure, close to P2B4's epicenter, partly due to deposition of eastward-propelled ejecta against the opposite (eastern) crater wall.

The subcrater structure at pad 2 (Fig. 7) showed visible disruption of layers extending to about the same level as the charge locations, consistent with previous experiments involving relatively shallow-scaled depths. Mixed fallback

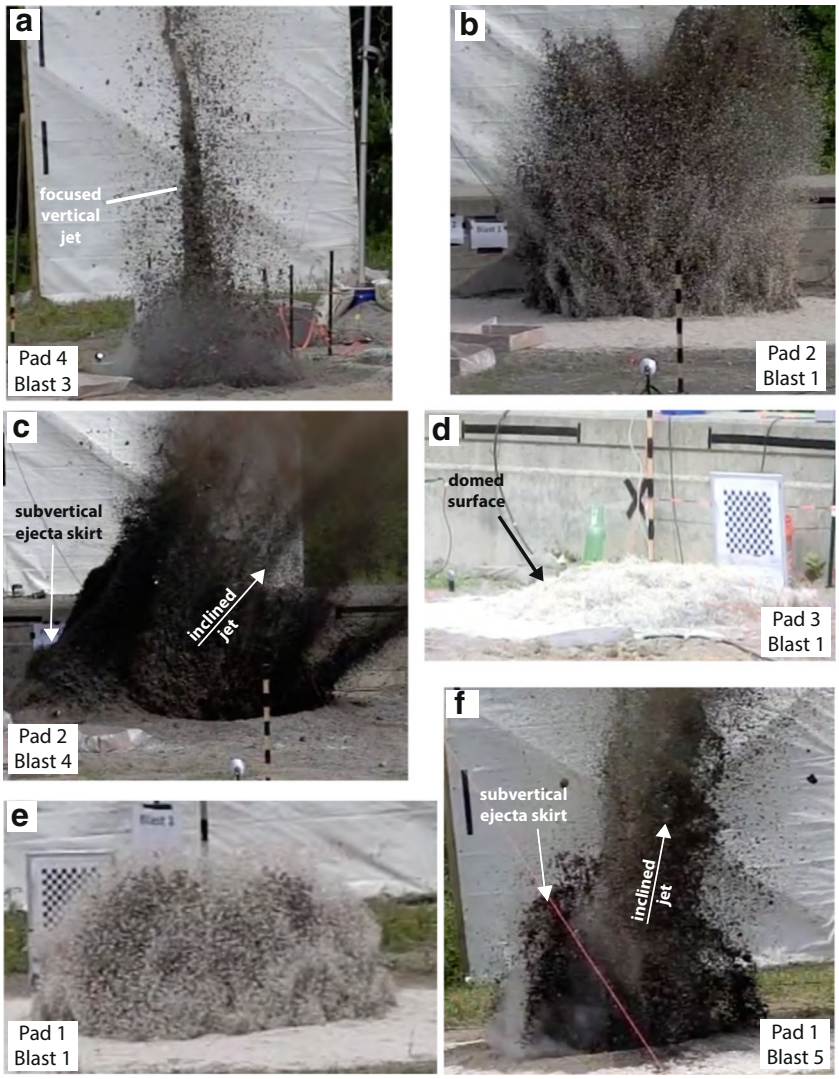

Fig. 4 Snapshots of blasts from high-speed videos at times at or near maximum ejecta jet heights. **a** Blast 3 at pad 4, illustrating vertically focused jet due to combination of deeper-than-optimal scaled depth and preexisting crater. *Black lines on white backdrop* are 50-cm long. Video available at Online Resource 1. **b** Pad 2, blast 1 showing a low-energy, symmetric jet with particle rich fingers, formed in the absence of a preexisting crater. Graduated stake in this and other photographs is marked at 10-cm intervals. Video at Online Resource 2. **c** Blast 4 at pad 2 showing inclined jet due to eruption from right (east) facing slope of preexisting crater and vertical skirt of ejecta. Video at Online Resource 3. **d** Pad 3, blast 1. Blast was fully contained, with no ejecta. Snapshot from instant of maximum height of updomed pad, which formed a hummocky surface as it fell back down. Video at Online Resource 4. **e** Ejecta jet during blast 1 at pad 1. This explosion was at or slightly shallower than the containment threshold and produced a very weak ejecta jet with maximum height (shown here) <1 m. *Checkerboard* pattern visible in photograph is 55 cm×55 cm. Video at Online Resource 5. **f** Pad 1, blast 5 ejecta jet, which is inclined toward the north (back and to right of plane of photograph) because the blast occurred beneath the north-facing slope of the preexisting crater wall. Note vertical skirt, which formed a thick ejecta deposit with limited lateral extent on the crater rim opposing the main jet direction. *Black line* on backdrop is 50 cm. Video at Online Resource 6

draped the entire crater. This deposit contained material from the three layers above the charge locations in the following proportions: 50 % sand, 30 % limestone screenings, and 20 % crushed asphalt in two samples and 100 % sand in a third. Note that these proportions reflect decreasing abundance of components from successively deeper layers of origin. The basal contact of mixed fallback was irregular and included subvertical contacts with domainal subcrater deposits. This reflects that mixed fallback and domainal subcrater deposits from one explosion became host material for subsequent explosions; thus, mixed fallback contributed domains to the domainal deposits. Domainal subcrater deposits were composed of materials originally above the charges, which were disrupted relative to their original flat layering and had irregular subhorizontal to subvertical contacts with each other. Within each domain, the material was pure or nearly pure, with only minimal mixing with other pad materials. The crater profile along the long axis shows that the crater was steepest

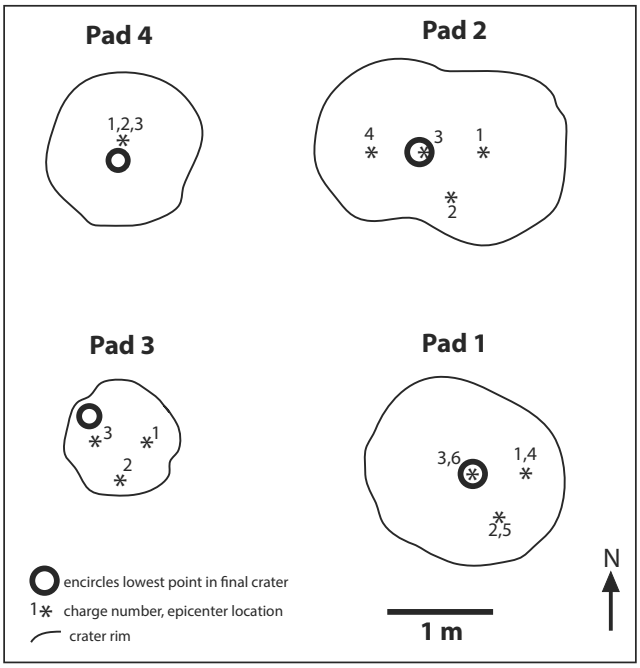

Fig. 5 Shapes of final crater rims with low point in each crater indicated as well as blast epicenters, shown in order of discussion in text (note that pad 3 is a subsidence pit rather than an excavated crater). Crater rims are defined by high points around craters as determined from photogrammetry

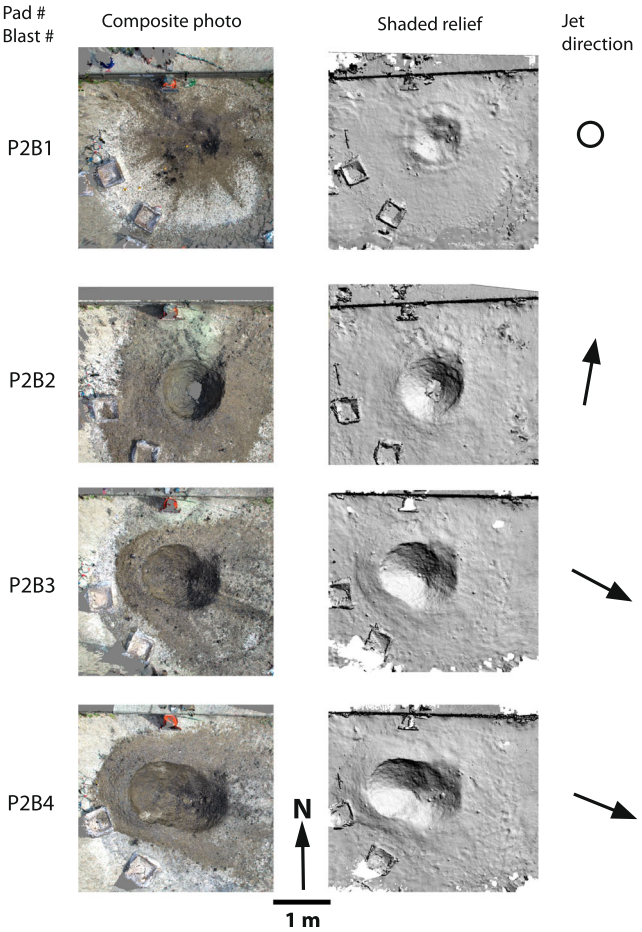

Fig. 6 Plan view composite, orthorectified photographs and shaded relief images from photogrammetry of pad 2 crater after each blast. *Circles* and *arrows* on right side represent vertical jets or directions of inclined jets, respectively. *Square* features are sample collection boxes. Note symmetric distribution of ejecta rays after blast 1. Blast 2 was centered under north-facing wall of crater from previous blast and produced a northward-inclined jet. Green sand on north side of crater had been emplaced around the charge. Blasts 3 and 4 produced southeast-inclined jets, which distributed ballistic clasts up to 20 m in that direction. Note thick but narrow ejecta ring around left (west) side of crater, which was deposited from the subvertical ejecta skirts associated with the inclined jets (see Fig. 4f)

on the west side, near the final blast (Fig. 8a), partly due to P2B4's inclined ejecta jet having deposited material onto the opposite side of the crater. The slightly elevated western rim was caused by deposition from a small subvertical skirt of ejecta around the edge of the main, inclined jet. Visibly disrupted subcrater materials (disrupted relative to their original layering) formed a broad but shallow zone and were thickest beneath the eastern part of the crater (Fig. 8a). We infer that that part of the pad was repeatedly disturbed by the initial triangular arrangement of blasts, while the western side only experienced one blast (blast 4). Interestingly, the penetration profile indicated deeper, albeit non-visible, disruption beneath the western side of the crater. It is possible that pad material that was disrupted (porosity increased) by preceding charges was re-compacted by the final charge to produce the asymmetry; similar data have arisen in other experiments but are still under evaluation.

Pad 3—lateral migration only, contained blasts

Pad 3 had three charges, each 80-cm deep relative to the original surface, arranged in the horizontal plane in an equilateral triangle with 50-cm sides (Table 1), with the objective of exploring the effects of laterally migrating, but non-erupting, explosions. With each blast, the pad surface domed upward around the epicenter (Fig. 4d, Online Resource 4) and then collapsed to form a low-relief (~2–5 cm) hummocky surface with a small central depression caused by subsidence. Successive, laterally offset blasts (P3B2, P3B3) simply enlarged the hummocky area (Fig. 9). The low point in the final, approximately circular structure (Table 1) was slightly offset from P3B3 epicenter (Fig. 5). The hummocky surfaces differed from the deepest blasts reported by Graettinger et al. (2014), which had deeper-scaled depths (0.011 m $J^{-1/3}$ compare with Table 1) and resulted in a slightly uplifted, but smooth, area around each epicenter with a sharply defined central collapse pit. The difference is because the current configuration is closer to the containment threshold than the earlier work.

Subcrater structures for pad 3 (Fig. 10) also differed from those produced by the deeper blasts, which were dominated by simple subsidence of pad layers (Graettinger et al. 2014).

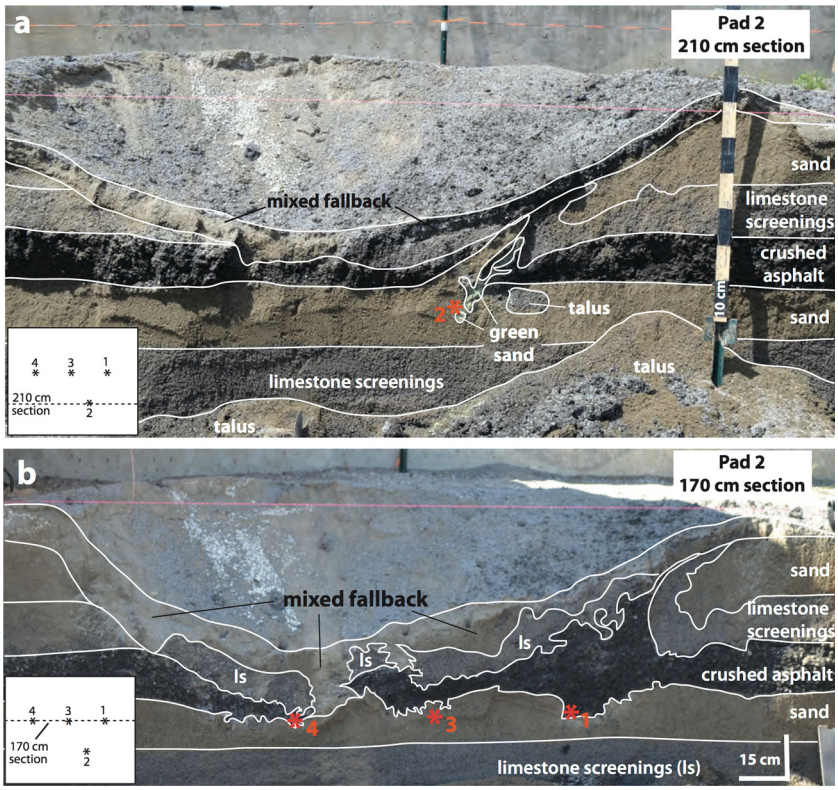

Fig. 7 Excavated cross sections through pad 2. Section locations measured from north edge of pad. *Insets* are plan views of the pad (north is up) with blast epicenters (*asterisks*) and line of cross section indicated (*dashed line*). **a** Cross section through location of charge 2 (*red asterisk*). **b** Cross section through locations of charges 1, 3, and 4. Note irregularly shaped domains of pad materials that originated above the charge locations. Domains are essentially "pure" and unmixed. Mixed fallback, in this case dominated by sand (probably from the topmost layer), drapes the crater

With lower confining forces, upward transport of pad materials had important effects even though no material was ejected. Pad layers originally above the charge locations were distorted into irregularly shaped domains that recorded downward displacement in the outer parts of the visibly disrupted zone and dominantly upward displacement in the central parts. Domains of different pad layer material, but with little or no internal mixing with other materials, had complex subvertical contacts with surrounding domains. Most subvertical domains remained "connected" to their original layers, but some subdecimeter-sized domains were isolated within other continuous domains (for example, small lenses of limestone screenings or crushed asphalt within a continuous sand domain; Fig. 10b). A sample from the uppermost few centimeters of the structure contained 90 % sand and 10 % limestone screenings, indicating that upward transport of the latter had produced some mixing during updoming and subsequent collapse of the ground surface (note that the change in behavior from purely contained explosions to those that eject material to produce fallback is a transitional one). The cross section through P3B2's location (Fig. 10a) likely illustrates the effects of a single blast, while the cross section through P3B1 and P3B3 illustrates superimposed effects of two closely spaced blasts (Fig. 10b). Colored sands that were used to fill the vertical, cylindrical charge emplacement holes provide useful markers for the subsurface blast effects. These sand columns were disintegrated either into grains diffusely mixed with host materials or into small centimeter-scale domains (e.g., small domain of orange sand; Fig. 10a) at locations between the charge and ~40 cm above the charge. They were not greatly displaced with respect to their original horizontal locations closer to the pad surface but were distorted by motion and interaction with surrounding materials. Below the original charge locations, they were scarcely affected (e.g., green sand in Fig. 10b). The penetration profile roughly parallels the profile of visible disruption, suggesting that blast effects extended in an envelope ~20 cm around the visible effects even though no permanent displacement of materials occurred within this envelope (Fig. 8b).

Pad 1—vertical and lateral migration, deep and shallow eruptive blasts

Pad 1 had the most complex charge configuration and probably most closely approached natural maar-diatreme conditions. The pad involved six blasts, the first three (70–75-cm deep) within ±4 % of the D_{sc}≈0.008 m $J^{-1/3}$ containment threshold and in a triangular plan-form configuration, while the next three were 50-cm deep relative to the original pad surface with the same triangular pattern of epicenters (Table 1). The first blast (Fig. 4e, Online Resource 5) threw out a small volume of material that mostly fell back onto the epicenter and extended ~30 cm radially outward; the resulting crater was subdued with a hummocky interior and vertical relief less than ~10 cm (Fig. 11). P1B2, with a slightly larger scaled depth due to a small difference between intended location and actual

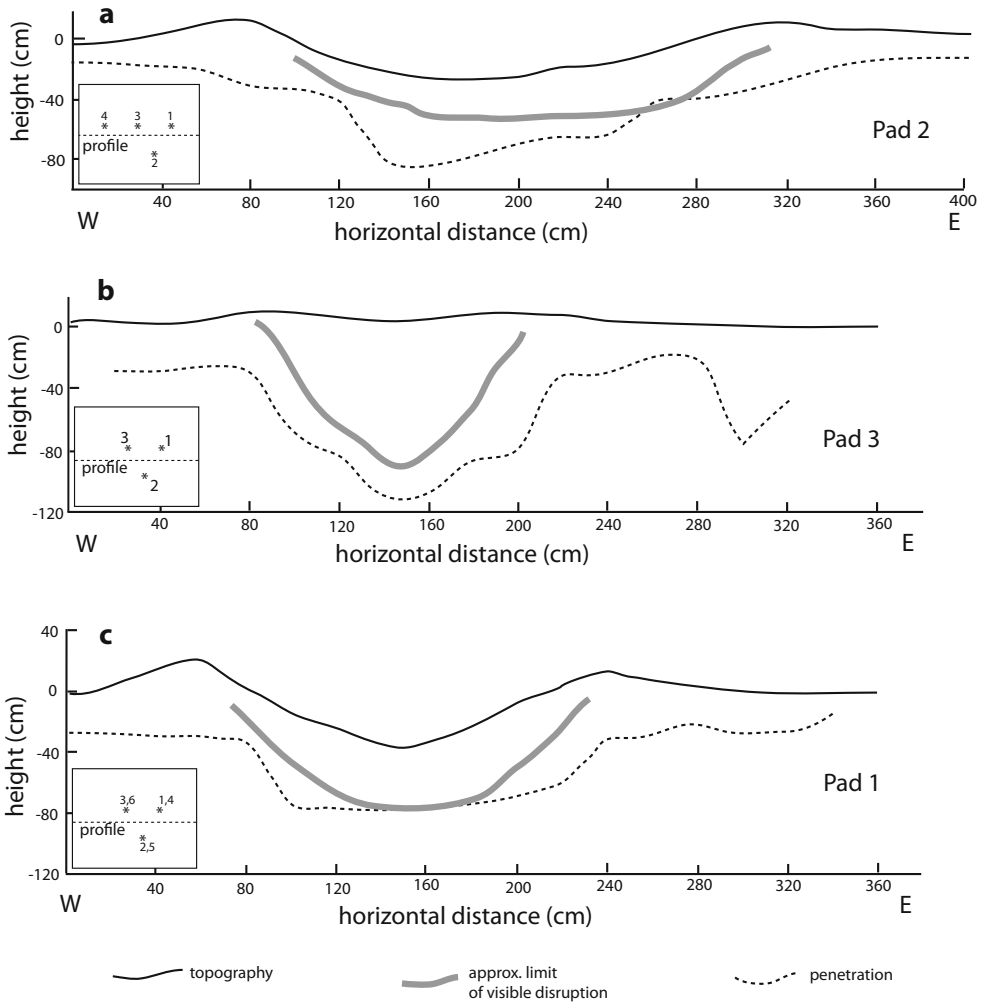

Fig. 8 Diagrams showing topographic profile, base of visually disrupted zone in subsurface, and depth of probe penetration through center of pads 2, 3, and 1 (**a**, **b**, and **c**, respectively). *Insets* are plan views of the pad (north is up) with blast epicenters (*asterisk*) and line of cross section indicated (*dashed line*). Note that the profiles were measured through the centers of the charge triangles, between the two cross sections shown in Figs. 7, 10, and 12. Probe penetration depths outside margins of craters are representative of pre-explosion values across each pad (note the anomalously large penetration depth in pad 3 at ~300 cm distance likely records a high porosity pocket that was not sufficiently compacted during pad construction and is not related to explosion effects)

charge depth, was transitional in behavior to the blasts at pad 3, ejecting a very small amount of material and mainly producing a hummocky surface within the slight depression of P1B1 (Fig. 11). The third blast was similar to P1B2. The landform that resulted from the first three, deeper blasts was a low relief, hummocky area with a small central depression, surrounded by a small amount of ejecta from blast 1 (Fig. 11). The fourth blast reoccupied the P1B1 epicenter but with a scaled depth between the optimal excavation and containment threshold values (Table 1). It made a small, 32-cm-deep crater surrounded by a narrow ejecta ring with distinct fingers of debris extending outward (Fig. 11). P1B5 was beneath the north-facing crater wall and ejected most material in a northward-directed, inclined jet (Figs. 4f, 11, Online Resource 6). This blast added slightly to the overall thickness of the P1B4 ejecta ring, but three short, prominent rays of debris extended from the southern half of the crater rim, deposited from a subvertical skirt around the inclined jet. The final charge was placed beneath the east-facing inner crater slope and ejected most material eastward in an inclined jet while again adding a small amount to the overall thickness of the ejecta ring (Fig. 11). The final pad 1 crater was slightly elongated, and its lowest point (42-cm deep; Table 1) coincided with the epicenter of the final blast (Fig. 5).

The subcrater deposits at pad 1 combined characteristics of those at pads 2 ("eruptive") and 3 ("non-eruptive"). The final crater was ~40-cm deep and draped with mixed fallback deposits in irregular contact with underlying domainal deposits, similar to pad 2 (Fig. 12). However, parts of pad 1's mixed fallback were visibly enriched in clasts derived from the upper limestone screenings and crushed asphalt layers, rather than being dominated by sand derived from the top pad layer as in pad 2. The composition of mixed fallback was quite varied, ranging from nearly pure sand (visual estimate) to one sample that was 16 % sand, 7 % limestone screenings, and 77 % crushed asphalt. The latter, crushed asphalt-enriched, fallback occurred on the crater wall above an asphalt domain that had been displaced upward relative to its original position in the pad (above location of charge 4 on Fig. 12b). This variability likely reflects a type of explosive mixing in which explosions

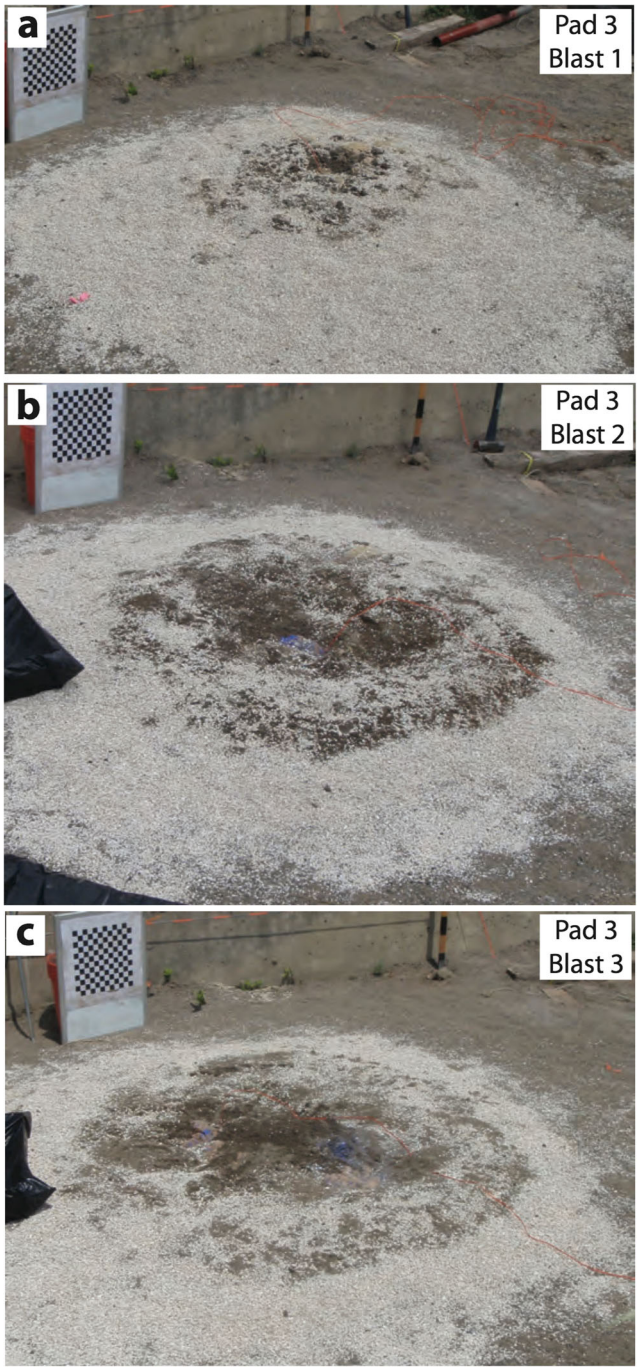

Fig. 9 Pad 3 surface after **a** blast 1, **b** blast 2, and **c** blast 3. All three blasts were fully contained but formed a hummocky pad surface as the updomed material collapsed (see Fig. 3d). The center of the hummocky surface featured a depression produced by subsidence. *Checkerboard* pattern visible in photographs is 55 cm × 55 cm, and concrete wall is to the north of the crater

ejected material that was displaced upward in the domainal subcrater deposits from previous blasts. Domainal deposits within the subcrater structure extended downward from the base of the mixed fallback to the level of charge emplacement. Similar to other experiments, these were characterized by an outer collar of downward-displaced layers and a central part

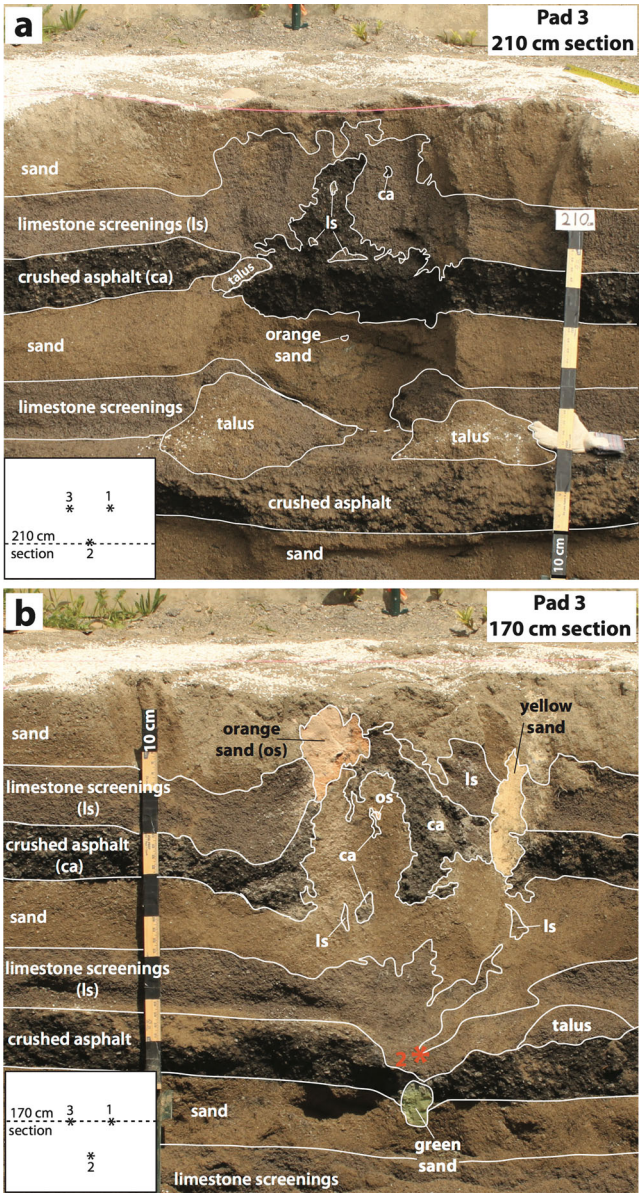

Fig. 10 Excavated cross sections through pad 3. Section locations measured from north edge of pad. *Insets* are plan views of the pad (north is up) with blast epicenters (*asterisks*) and approximate lines of cross section indicated (*dashed line*). Slumping of the face during excavation, because pad materials had been weakened by repeated explosions, means that the faces are not flat. In cross section **a**, the *upper part* (above the lower crushed asphalt layer) is exposed at ~210 cm, through the line of charge 2. Charge 2 was emplaced in the lower asphalt layer; thus, its location is not yet exposed in **a**. The *lower part* of cross section **b** cut through the charge 2 location, but the *upper part* is the plane through charges 1 and 3. Colored sands were emplaced around the charges, extending ~5 cm below the charges and to the top of the emplacement holes (level with pad surface); *yellow* for charge 1, *green* for charge 2, and *orange* for charge 3. Note subvertical domains of essentially pure pad materials with irregular contacts. Partial subsidence collar can be seen in **b** on the left side of the subsurface structure. Small domains of limestone screenings and crushed asphalt record breaking up of domains by successive blasts. Domains experienced net vertical displacement even though there was no "eruption." Blasts were located a few centimeters below the containment threshold

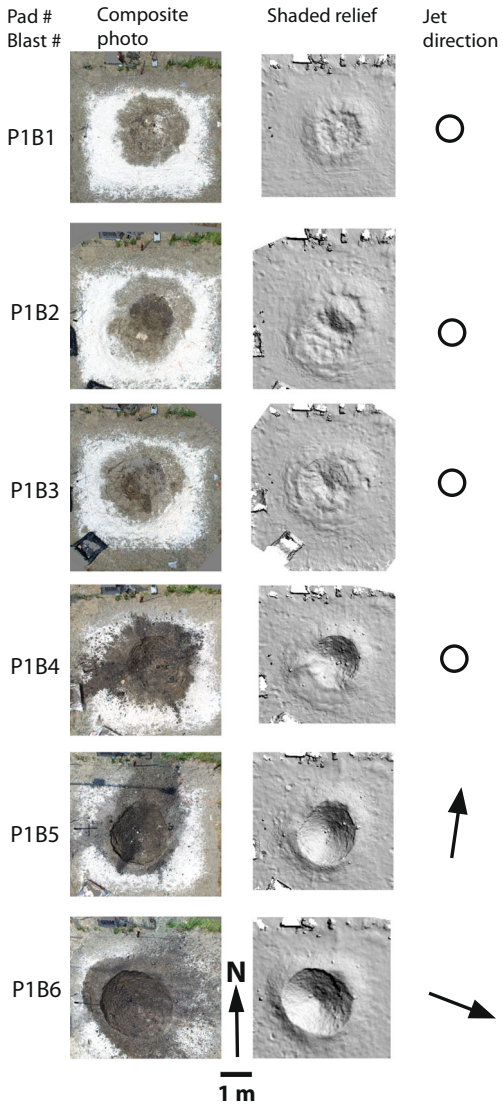

Fig. 11 Plan view composite, orthorectified photographs, and shaded relief images from photogrammetry of pad 1 crater after each blast. *Circles* and *arrows* on right side represent vertical jets or directions of inclined jets, respectively. *Square* features are sample collection boxes. Blasts 1–3 were just shallower than, or at, the containment threshold (see Fig. 4e), with the first one producing a small quantity of ejecta and a hummocky surface that was expanded by blasts 2 and 3. Blast 4 produced a symmetric, but rayed, ejecta deposit. Blasts 5 and 6 produced inclined jets first to the north (Fig. 4f) and then to the east

with irregularly shaped domains of pure pad materials with complex contacts. As with pad 3, most domains could be traced continuously into undisturbed pad layers, but some subdecimeter-sized domains were isolated within other materials (e.g., Fig. 12b); this probably records progressive breakdown of domains with repeated explosions and inclusion of mixed fallback from early explosions into domains by later blasts, as mentioned above. The smaller domains were of mixed composition, supporting the latter scenario; examples of such smaller domains are those just above the P1B6 charge location (Fig. 12b), which contained nearly equal parts limestone screenings and crushed asphalt. Small 2–3-cm domains of colored sands from emplacement holes were observed in the deep part of the structure (Fig. 12), but unlike at pad 3, the upper parts of the colored sand fills were blown out of the crater. The penetration profile roughly parallels the zone of visible disruption (Fig. 8c).

Once post-shot excavations had exposed the northern edge of the epicenter triangle (the P1B1, 4–P1B3, 6 plane), further excavation exposed a horizontal surface at a depth of ~40 cm relative to the original pad surface, i.e., just at the bottom of the crater. This plan view illustrates the crudely concentric organization of domains within the subcrater structure, with mixed fallback in the center (Fig. 13).

Discussion

Multiblast craters

In order to understand the relations between final crater shape after laterally shifting explosions, it is useful to define a reference crater footprint that is a measure of the area of surface disruption that could be caused by each individual explosion if it occurred beneath flat ground. The footprint is based on the diameter (m) of the maximum reference crater, which is estimated as $d_{ref}=(0.014\ \text{m}\ \text{J}^{-1/3})\cdot E^{1/3}$. It is a maximum crater diameter for energy E because it is empirically derived for explosions at optimal scaled depth ($D_{sc}=0.004\ \text{m}\ \text{J}^{-1/3}$; Goto et al. 2001). For the explosions reported here, $d_{ref}=1.3$ m.

Pads 1 and 2 provide insight that can be extended to natural craters produced by laterally shifting "erupting" explosions (as opposed to pad 3 where all blasts were contained). At pad 1, each blast was within the footprint of the preceding blasts' reference craters, and the final crater was approximately circular in shape. The final crater was centered on the epicenter of the last of the six blasts, rather than coinciding with the center of the triangular epicenter pattern. This suggests that successive blasts that have epicenters within the footprints of preceding blasts can enlarge the crater and shift its center while maintaining a roughly circular shape. Shifting of the center location also partly resulted from the fact that, for explosions such as those at pad 1, which are deeper than optimal excavation depth, much of the ejecta fall back into the crater or onto a proximal ejecta ring. Thus, subsequent blasts at pad 1 partially refilled the preceding crater beneath which they occurred (Fig. 14) so that the final landform is centered on the final blast. The inclined ejecta jets for blasts 5 and 6 deposited material onto the opposite walls, enhancing this effect.

Pad 2 produced a compound, elongated crater, probably because blast 4 was outside the reference footprints of blast 1 and, to a lesser degree, blast 2 (Fig. 14). This suggests that when lateral shifting of explosion sites causes an epicenter to

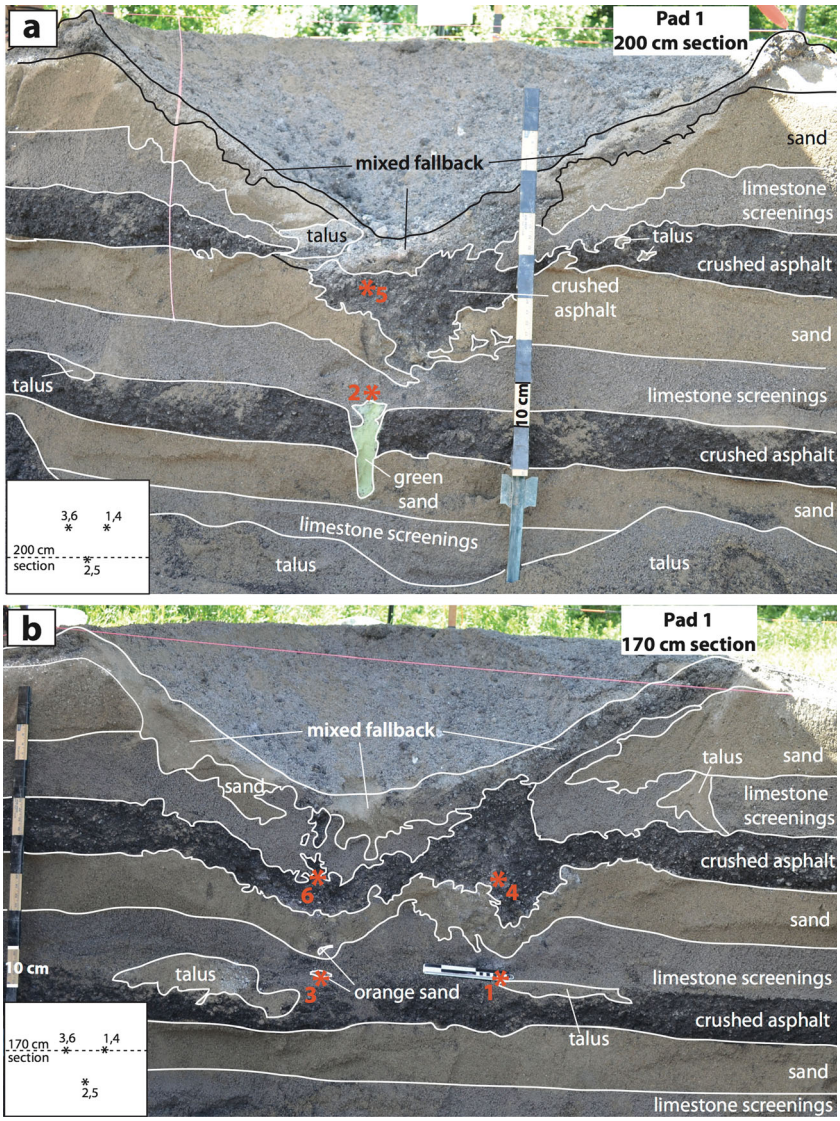

Fig. 12 Excavated cross sections through pad 1. *Insets* as in previous cross sections. **a** Cross section through locations of charges 2 and 5. Green sand was originally emplaced below, around, and as a fill of the charge 2 hole; that shown in the cross section was below the charge. **b** Cross section through locations of charges 1, 3, 4, and 6. Small domains above charge 6 location are of mixed composition. Note subsidence around central subcrater structure which has complex domains with irregular boundaries

be outside the footprints of preceding blasts, but is close enough that the footprints of the preceding and new explosions overlap, the new blast's crater will overlap with the previously formed one to form an elongated or compound crater. Obviously, if the new explosion epicenter is sufficiently far from the existing crater that their footprints do not overlap, the result will be two separate craters.

Formation of subcrater deposits

Ross et al. (2013) and references therein described the role of explosion phenomena in producing different types of subcrater deposits in terms of five main stages, which are useful to review before discussing the experimental results. (1) Detonation produces a high-pressure gas bubble that in turn causes a stress wave to propagate into the surrounding media. (2) The stress wave accelerates particles upward as it reflects off the ground surface, causing the ground to dome up around the explosion epicenter. (3) Expansion of the gas bubble, accentuated in the upward direction (toward low pressure at the ground surface), continues to push the surface dome upward. (4) Gas bubble expansion and venting disaggregate the surface dome and send near-surface particles on ballistic trajectories while opening up a transient crater. Deeper-seated materials (but above the explosion site) experience a shorter time of acceleration, are not lofted as far, and fall back sooner with little or no lateral displacement to form deposits with pure domains. These deposits are enveloped by cryptic fallback that is not visibly disrupted but was moved slightly and loosened within the transient cavity (Ross et al. 2013). (5) Surrounding materials flow/subside into the transient cavity and some lofted material falls back into it, with the end result being

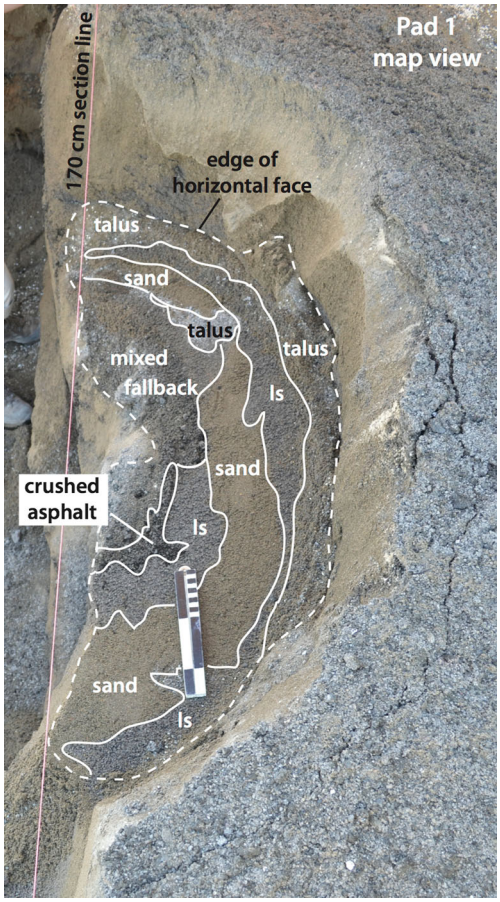

Fig. 13 Plan view excavation of part of the pad 1 subcrater structure showing crudely concentric arrangement of domains. Left edge of excavation corresponds to the face shown in Fig. 11b. Horizontal cut is a few centimeters above the lowest part of the final pad 1 crater. Symbol *ls* is limestone screenings

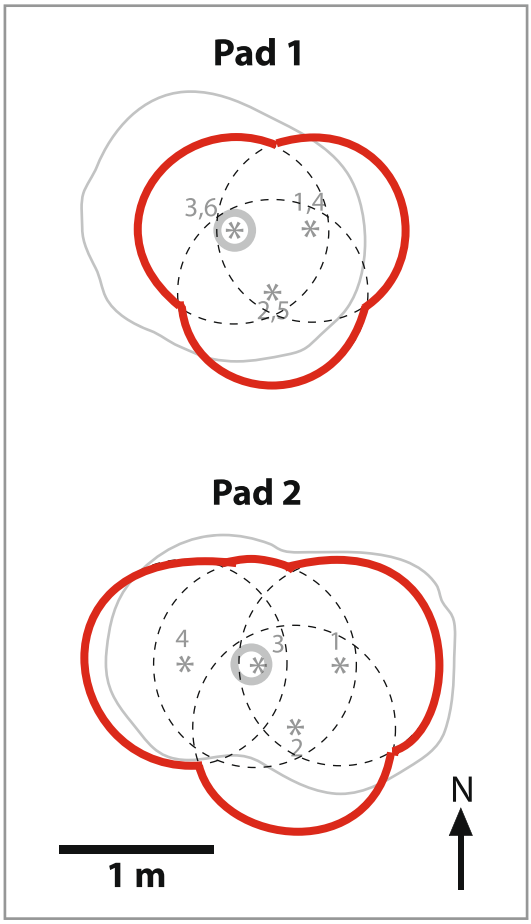

Fig. 14 Comparison of a crater shaped by simple overlapping craters (*red*) compared to actual crater shapes (*gray*, from Fig. 5), for pads 1 and 2. Each *dashed circle*, representing the reference footprint of an explosion, has a diameter of 1.3 m, which corresponds to the maximum single explosion crater diameter predicted by Goto et al. (2001). Other symbols are the same as Fig. 5

the final crater. Apparently subsided materials around the edge of visible disruption may have also experienced upward transport before falling back onto the transient crater floor but without being disassembled. During stage 5, flowing materials can converge at the center-bottom of the transient cavity and can form an upward-directed jet, referred to as a granular fountain, that may be partly preserved as a vertical column with a consistent composition as the transient crater relaxes (Andrews et al. 2014). Stages 4 and 5 overlap in time, and both contribute to the formation of domainal subcrater deposits. Note that these processes apply to "erupting" explosions, whereas in fully contained explosions (D_{sc}>0.008 m·$J^{-1/3}$), the gas bubble does not vent but disperses into the surrounding media and partly condenses on grain surfaces (in our experiments, the latter produces an explosives residue on pad materials, whereas in phreatomagmatic cases, the condensate would be liquid water within the evolving diatreme).

The experiments reported here produced subcrater deposits with characteristics similar in some ways to those of previous experiments without lateral explosion migration. In the eruptive cases, mixed fallback overlays domainal subcrater deposits. In most single and multiple eruptive explosion cases with only vertical blast migration (Ross et al. 2013; Graettinger et al. 2014), the domainal subcrater deposits feature a variably developed collar of downward-displaced material around a core zone with irregular, subvertical, crosscutting contacts. Material from the pad layer corresponding to the level just above the shallowest explosions typically forms a central domain that extends upward to the base of mixed fallback. Thus, the domainal subcrater deposits tend to form an annular pattern in map view (Fig. 15), with the outer part recording net subsidence (stratigraphically higher host material moving inward from the annulus edge), while the inner part preserves net upward displacement of material (stratigraphically deeper host material toward the annulus center). As noted by Ross et al. (2013), the crosscutting relations and net upward displacement are not the result of simple upward intrusion of deeper-seated material but from brief lofting of material in the transient cavity and fallback as pure, but

partly disassembled, domains and/or by the granular fountaining process (Andrews et al. 2014).

Pads 1–3 (Figs. 7, 10, and 12) show that beneath mixed fallback deposits is a variably developed collar of downward-displaced material surrounding an inner zone that is dominated by domains with complex crosscutting relations at a variety of angles. These domains represent overlapping effects of individual explosions. For example, the first explosion at a pad might produce subcrater deposits similar to the idealized example in Fig. 15. The next explosion, offset to the right or left of the first one but beneath the crater, causes a similar combination of outer downward-displaced and inner crosscutting contacts and upward displacement. However, its "starting materials" were not simple layers but rather the subcrater structure produced by the first explosion. These overlapping effects continue with subsequent explosions to produce complex structures seen in pads 1–3. A horizontal cut through pad 1 (Fig. 13) revealed domains that were crudely organized in a concentric pattern around the site of the last explosion (P1B6). Some of these domains were not continuous but instead were the tops of subvertical domains from preceding blasts.

In nature, we expect that the potentially large number of phreatomagmatic or/and hydrothermal explosions at an eruptive center would result in complex, crosscutting domains

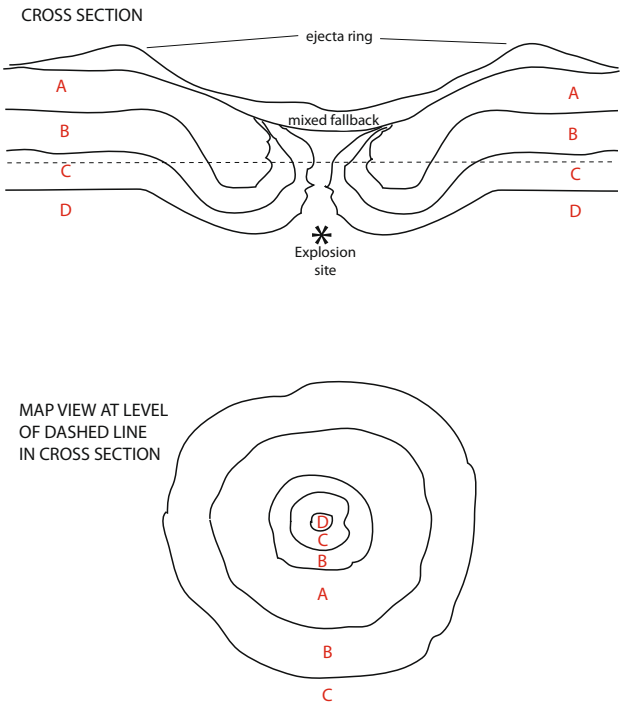

Fig. 15 Cross section (*top*) and plan view at level of *dashed line* (*bottom*) of simplified subcrater structure produced by a single explosion at scaled depth less than the containment threshold but deeper than the optimal crater excavation scaled depth. Multiple explosions can produce similar structures if their locations only vary in the vertical dimension. A laterally offset explosion in similar scaled depth range would use this configuration as the starting material that leads to the new subcrater structure

with subvertical contacts within a variable-width collar of downward-displaced host materials that may exhibit centroclinally dipping beds. Once a diatreme has developed, the host materials for a given explosion include materials within the diatreme itself, not just the surrounding country rocks. Thus, the experiments suggest that deeper levels of a mature diatreme would contain material that was originally higher in the diatreme, including material that had been erupted earlier and deposited on the crater floor or on the proximal parts of a tephra ring that later collapsed into the crater. These expectations are consistent with field data from diatremes (e.g., Brown et al. 2008; LeFebvre et al. 2013; Gernon et al. 2013; Delpit et al. 2014).

Two final issues relate to mixing processes in maar-diatremes and comparison with fluidization-based conceptual models for diatremes and kimberlite pipes. Recent papers have emphasized the role of mixing in diatremes through repeated subsurface explosions (Ross and White 2006; White and Ross 2011; Valentine 2012; Valentine and White 2012; LeFebvre et al. 2013; Gernon et al. 2013). This mixing process is thought to be the mechanism by which deep-seated country rock fragments are brought to shallow levels where they can be ejected by shallow, eruptive explosions with shallow-scaled depths (Valentine 2012; LeFebvre et al. 2013; Graettinger et al. 2014; Valentine et al. 2014). The current experiments demonstrate that, at the shallowest levels, mixing occurs during ballistic ejection of material as the explosive gas bubble vents; this shallow material is completely disaggregated and mixing occurs in the eruptive jet and during sedimentation as fallback or onto the tephra rim. Repeated explosions at depth cause net upward displacement of some pure domains until they extend to the shallowest levels where their materials can be ballistically ejected. At deeper levels, mixing occurs through progressive breakdown of domains within the domainal subcrater deposits. Recurring explosions break up the domains until their size is similar to the size of the irregularities along the edges of pure domains (see description of pad 1), at which point the smallest domains become mixtures. This process appears to be enhanced by lateral shifting of explosion sites.

Subsurface explosions produce many of the characteristics of diatremes and kimberlite pipes that have been attributed to gas-driven fluidization (e.g., Woolsey et al. 1975; Walters et al. 2006; Gernon et al. 2008; Gernon et al. 2009), including downward slumping of outer materials (collar) around more massive deposits with subvertical contacts. Fluidization refers to situations of partial or complete particle support due to sustained upward flux of an interstitial gas, which is normally considered to be magmatic volatiles, particularly in the kimberlite literature. Gernon et al. (2009) suggested that phreatomagmatic processes would also cause fluidization processes via resulting steam flow. However, the dynamics of discrete subsurface explosions are not generally analogous to

fluidization sensu stricto. Rather, the formation of massive domains with subvertical contacts and outer slumping structures in discrete explosions is related to expansion and venting (unless a blast is deeper than the containment threshold) of a gas bubble, lifting and fallback during transient crater opening and collapse, and granular jets or fountains (Ross et al. 2008a, b; Ross et al. 2013; Andrews et al. 2014). During fallback, the particles are not supported at all, and the process cannot be considered a fluidization of any sort. While the end results may appear similar to those produced in fluidization experiments, the processes are quite different.

Conclusions

Many, if not most, phreatomagmatic and hydrothermal explosion craters and underlying diatremes are the result of multiple subsurface explosions centered at different depths and/or lateral locations. Previous experiments and a new one reported here with only vertical variation in explosion sites have demonstrated that the landforms and subsurface structures can result from an interplay between explosion energy, scaled depth, the effects of preexisting craters on ejecta jets, and whether an explosion is fully contained or is able to vent. Experiments with laterally shifting explosion sites indicate that final crater shape depends upon the location of explosion epicenters relative to the empirically predicted, single-blast reference crater footprint for each individual blast. Experimental subcrater deposits illustrate the complexity of overlapping structures and how this can facilitate different mechanisms for mixing materials within very shallow and deep parts of the structures. The structures that result from discrete subsurface explosions are similar in general characteristics to those produced by fluidization experiments, but the mechanisms for generating those structures are very different.

Current work is exploring the effect of host material properties on craters, ejecta, and subsurface structures. As noted above, a large body of experimental data indicates that material properties generally have second-order effects on major parameters such as crater diameter and on transitions in explosion behavior as a function of scaled depth. The most significant affects of host properties are probably on the details of crater morphology (e.g., steepness of walls) and on the clast sizes available for ejection. Note that once subsurface explosions begin to disrupt a host material, its original strength has less impact on subsequent processes. Additionally, in natural maar-diatremes, much of the disrupted subsurface structure is never empty but rather is filled with debris and juvenile material; this explains why diatremes hosted by soft host material have steep sides as do those hosted hard rocks (see discussion in Delpit et al. 2014); only the very shallow part that is open to the air (i.e., the crater) is likely to be strongly affected by material strength due to slumping of crater walls both during and after eruptive activity.

Natural maar-diatremes are likely to result from tens to thousands of discrete explosions, many of which have localized effects compared to the size of the final structure at the end of an eruptive episode. Thus, the experiments reported here are most directly related to the early phases of maar-diatreme development (see also Ross et al. 2013). We expect that explosion phenomena will be similar in a mature diatreme compared to a newborn one, but materials may be better mixed and subsidence and slumping may be more extensive. It probably is not practical to experimentally reproduce the effects of such large numbers of blasts. Future work should focus on exploring focused questions that have arisen from the experiments to date (Valentine et al. 2012; Taddeucci et al. 2013; Ross et al. 2013; Graettinger et al. 2014; this paper), such as multiparameter empirical relationships that can provide better energy and ballistics estimates for hazard assessment.

Acknowledgments This work was partly supported by the US National Science Foundation (EAR 1420455 to Valentine) and by the 3E fund at University at Buffalo. JDLW acknowledges support from MBIE, New Zealand. Additional contributions from J. Taddeucci, D. Bowman, J. Lees, A. Harris, and M. Bombrun are gratefully acknowledged. Valuable assistance was provided by B. Catalano, P. Johnson, J. Krippner, T. Larson, T. Macomber, S. Morealli, P. Moretti, E. Panza, R. Rodd, D.S.C. Ruth, R. Wagner, M. Williams, J. Wilczak, D. Klingensmith, B. Pitman, and C. Mitchell. We thank M. Ort and U. Kueppers for their helpful reviews of the manuscript.

References

Andrews RG, White JDL, Dürig T, Zimanowski B (2014) Discrete blasts in granular material yield two-stage process of cavitation and granular fountaining. Geophys Res Lett 41:422–428. doi:10.1002/2013GL058526

Begét JE, Hopkins DM, Charron SD (1996) The largest known maars on Earth, Seward Peninsula, northwest Alaska. Arctic 49:62–69

Bowman DC, Taddeucci J, Keehoon K, Anderson JF, Lees JM, Graettinger AH, Sonder I, Valentine GA (2014) The acoustic signatures of ground acceleration, gas expansion, and spall fallback in experimental volcanic explosions. Geophys Res Lett 41:1916–1922. doi:10.1002/2014GL059324

Breard ECP, Lube G, Cronin SJ, Fitzgerald R, Kennedy B, Scheu B, Montanaro C, White JDL, Tost M, Procter JN, Moebis A (2014) Using the spatial distribution and lithology of ballistic blocks to interpret eruption sequence and dynamics: August 6 2012 Upper Te Maari eruption, New Zealand. J Volcanol Geotherm Res 286:373–386. doi:10.1016/j.jvolgeores.2014.03.006

Brown RJ, Gernon T, Stiefenhofer J, Field M (2008) Geological constraints on the eruption of the Jwaneng Centre kimberlite pipe, Botswana. J Volcanol Geotherm Res 174:195–208. doi:10.1016/j.jvolgeores.2007.12.032

Carrasco-Núñez G, Ort MH, Romero C (2007) Evolution and hydrological conditions of a maar volcano (Atexcac crater, Eastern Mexico). J Volcanol Geotherm Res 159:179–197

Christiansen RL, Peterson DW (1981) Chronology of the 1980 eruptive activity. In: Lipman PW, Mullineaux DR (eds) The 1980 eruptions of Mount St. Helens, Washington. US Geol Surv Prof Pap 1250, pp. 17-30

Delpit S, Ross P-S, Hearn BC (2014) Deep-bedded ultramafic diatremes in the Missouri River Breaks volcanic field, Montana, USA: 1 km of syn-eruptive subsidence. Bull Volcanol 76:832. doi:10.1007/s00445-014-0832-8

Gernon TM, Gilbertson MA, Sparks RSJ, Field M (2008) Gas-fluidisation in an experimental tapered bed: insights into processes in diverging volcanic conduits. J Volcanol Geotherm Res 174:49–56. doi:10.1016/j.jvolgeores.2007.12.034

Gernon TM, Gilbertson MA, Sparks RSJ, Field M (2009) The role of gas-fluidisation in the formation of massive volcaniclastic kimberlite. Lithos 112:439–451. doi:10.1016/j.lithos.2009.04.011

Gernon TM, Upton BGJ, Hinks TK (2013) Eruptive history of an alkali basaltic diatreme from Elie Ness, Fife, Scotland. Bull Volcanol 75: 704. doi:10.1007/s00445-013-0704-7

Goto A, Taniguchi H, Yoshida M, Ohba T, Oshima H (2001) Effect of explosions energy and depth to the formation of blast wave and crater: field explosion experiment for the understanding of volcanic explosion. Geophys Res Lett 28:4287–4290

Graettinger AH, Valentine GA, Sonder I, Ross P-S, White JDL, Taddeucci J (2014) Maar-diatreme geometry and deposits: subsurface blast experiments with variable explosion depth. Geochem Geophys Geosys 15, doi:10.1002/2013GC005198

Houser FN (1969) Subsidence related to underground nuclear explosions, Nevada Test Site. Bull Seism Soc Am 59:2231–2251

Jolly AD, Jousset P, Lyons JJ, Carniel R, Fournier N, Fry B, Miller C (2014) Seismo-acoustic evidence for an avalanche driven phreatic eruption through a beheaded hydrothermal system: an example from the 2012 Tongariro eruption. J Volcanol Geotherm Res 286:331–347. doi:10.1016/j/jvolgeores.2014.04.007

Jordan SC, Cas RAF, Hayman PC (2013) The origin of a large (>3 km) maar volcano by coalescence of multiple shallow craters: Lake Parrumbete maar, southeastern Australia. J Volcanol Geotherm Res 254:5–22. doi:10.1016/j.jvolgeores.2012.12.019

Kokelaar BP (2002) Setting, chronology and consequences of the eruption of Soufrière Hills Volcano, Montserrat (1995-1999). In: Druitt TH, Kokelaar BP (eds) The eruption of Soufrière Hills Volcano, Montserrat, from 1995 to 1999. Geol Soc Lond Mem 21, London, pp 1-43

Lefebvre N, White JDL, Kjarsgaard BA (2013) Unbedded diatreme deposits reveal maar-diatreme-forming eruptive processes: Standing Rocks West, Hopi Buttes, Navajo Nation, USA. Bull Volcanol 75: 739. doi:10.1007/s00445-013-0739-9

Lorenz V (1986) On the growth of maars and diatremes and its relevance to the formation of tuff-rings. Bull Volcanol 48:265–274

Lube G, Breard ECP, Cronin SJ, Procter JN, Brenna M, Moebis A, Pardo N, Stewart RB, Jolly A, Fournier N (2014) Dynamics of surges generated by hydrothermal blasts during the 6 August 2012 Te Maar eruption, Mt. Tongariro, New Zealand. J Volcanol Geotherm Res 286:348–366. doi:10.1016/j.jvolgeores.2014.05.010

Ohba T, Taniguchi H, Oshima H, Yoshida M, Goto A (2002) Effect of explosion energy and depth on the nature of explosion cloud: a field experimental study. J Volcanol Geotherm Res 115:33–42

Ort MH, Carrasco-Núñez G (2009) Lateral vent migration during phreatomagmatic and magmatic eruptions at Tecuitlapa Maar, east-central Mexico. J Volcanol Geotherm Res 181:67–77

Procter JN, Cronin SJ, Zernack AV, Lube G, Stewart RB, Nemeth K, Keys H (2014) Debris flow evolution and the evolution of an explosive hydrothermal system, Te Maar, Tongariro, New Zealand. J Volcanol Geotherm Res 286:303–316. doi:10.1016/j.jvolgeores.2014.07.006

Rooke AD, Carnes BL, Davis LK (1974) Cratering by explosions: a compendium and an analysis. Tech Rep N-74-1, U.S. Army Engineer Waterways Experiment Station, Vicksburg, Mississippi

Ross P-S, White JDL (2006) Debris jets in continental phreatomagmatic volcanoes: a field study on their subterranean deposits in the Coombs Hill vent complex, Antarctica. J Volcanol Geotherm Res 149:62–84

Ross P-S, White JDL, Zimanowski B, Büttner R (2008a) Multiphase flow above explosion sites in debris-filled volcanic vents: insights from analogue experiments. J Volcanol Geotherm Res 178:104–112

Ross P-S, White JDL, Zimanowski B, Büttner R (2008b) Rapid injection of particles and gas into non-fluidized granular material, and some volcanological implications. Bull Volcanol 70:1151–1168. doi:10.1007/s00445-008-0230-1

Ross P-S, White JDL, Valentine GA, Taddeucci J, Sonder I, Andrews RG (2013) Experimental birth of a maar-diatreme volcano. J Volcanol Geotherm Res 260:1–12. doi:10.1016/j.jvolgeores.2013.05.005

Taddeucci J, Valentine GA, Sonder I, White JDL, Ross P-S, Scarlato P (2013) The effect of pre-existing craters on the initial development of explosive volcanic eruptions: an experimental investigation. Geophys Res Lett 40:507–510. doi:10.1002/grl.50176

Valentine GA (2012) Shallow plumbing systems for small-volume basaltic volcanoes, 2: evidence from crustal xenoliths at scoria cones and maars. J Volcanol Geotherm Res 223–224:47–63. doi:10.1016/j.jvolgeores.2012.01.012

Valentine GA, White JDL (2012) Revised conceptual model for maar-diatremes: subsurface processes, energetics, and eruptive products. Geology 40:1111–1114. doi:10.1130/G33411.1

Valentine GA, White JDL, Ross P-S, Amin J, Taddeucci J, Sonder I, Johnson PJ (2012) Experimental craters formed by single and multiple buried explosions and implications for volcanic craters with emphasis on maars. Geophys Res Lett 39, L20301. doi:10.1029/2012GL053716

Valentine GA, Graettinger AH, Sonder I (2014) Explosion depths for phreatomagmatic eruptions. Geophys Res Lett 41:3045–3051. doi:10.1002/2014GL060096

van Otterloo J, Cas RAF, Sheard MJ (2013) Eruption processes and deposits characteristics at the monogenetic Mt. Gambier Volcanic Complex, SE Australia: implications for alternating magmatic and phreatomagmatic activity. Bull Volcanol 75:737. doi:10.1007/s00445-013-0737-y

Walters AL, Phillips JC, Brown RJ, Field M, Gernon T, Stripp G, Sparks RSJ (2006) The role of fluidization in the formation of volcaniclastic kimberlite: grain size observations and experimental investigation. J Volcanol Geotherm Res 155:119–137. doi:10.1016/j.jvolgeores.2006.02.005

White JDL (1991) Maar-diatreme phreatomagmatism at Hopi Buttes, Navajo Nation (Arizona), USA. Bull Volcanol 53:239–258

White JDL, McClintock MK (2001) Immense vent complex marks flood-basalt eruption in a wet, failed rift: Coombs Hills, Antarctica. Geology 29:935–938

White JDL, Ross P-S (2011) Maar-diatreme volcanoes: a review. J Volcanol Geotherm Res 201:1–29

Woolsey TS, McCallum ME, Schumm SA (1975) Modeling of diatreme emplacement by fluidization. Phys Chem Earth 9: 30–42